

Design strategy for ferroelectric-based polar metals with dimensionality-tunable electronic states

[Ma Chao](#) and [Jin Kuijuan](#)

Citation: [SCIENCE CHINA Physics, Mechanics & Astronomy](#) **61**, 097011 (2018); doi: 10.1007/s11433-018-9245-4

View online: <http://engine.scichina.com/doi/10.1007/s11433-018-9245-4>

View Table of Contents: <http://engine.scichina.com/publisher/scp/journal/SCPMA/61/9>

Published by the [Science China Press](#)

Articles you may be interested in

[Ground state and polaron and bipolaron excited states in polydiacetylene](#)

Science in China Series G-Physics, Mechanics & Astronomy **49**, 430 (2006);

[Purely organic optoelectronic materials with ultralong-lived excited states under ambient conditions](#)

Science Bulletin **60**, 1631 (2015);

[Electronic structure and magnetic properties of metastable SmCo₇ compound](#)

Science in China Series G-Physics, Mechanics & Astronomy **48**, 325 (2005);

[Theoretical study on stability and nonlinear optical properties of tetrahydropyrrole diradical and its isoelectronic systems in different electronic states](#)

SCIENCE CHINA Chemistry **54**, 1086 (2011);

[Synthesis and optoelectronic properties of amino-functionalized carbazole-based conjugated polymers](#)

SCIENCE CHINA Chemistry **56**, 1119 (2013);

Design strategy for ferroelectric-based polar metals with dimensionality-tunable electronic states

Chao Ma^{1,2}, and KuiJuan Jin^{1,2*}

¹ Beijing National Laboratory for Condensed Matter Physics, Institute of Physics, Chinese Academy of Sciences, Beijing 100190, China;

² School of Physical Sciences, University of Chinese Academy of Sciences, Beijing 100190, China

Received April 4, 2018; accepted May 14, 2018; published online July 10, 2018

Since LiOsO₃ was discovered, obtaining easy-accessible polar metals for research and applications has been challenging. In this paper, we present a multilayer design strategy, which is configured as ferroelectric layer/carrier reservoir layer/isolation layer/substrate, for obtaining polar metals by electrostatically doping a strained ferroelectric material in a more effective way. In the proposed configuration, both 1 unit-cell thick BaTiO₃ and PbTiO₃ exhibited considerable Ti off-centering with various strains, which should extend the applicability of ferroelectric-based polar metals in ultra-thin devices. Moreover, engineered by the compressive strain and the BaTiO₃ thickness, the design strategy effectively achieved polar metallicity and dimensionality-tunable electronic states associated with the modulation of highly anisotropic properties such as electrical and electronic thermal conductivity, which may be helpful for designing ultra-thin, ultrafast, and low-power switch devices.

polar metal, design strategy, BaTiO₃, highly anisotropic conductivity, electrical conductivity, electronic thermal conductivity

PACS number(s): 68.65.Ac, 71.20.-b, 71.18.+y, 72.15.Eb

Citation: C. Ma, and K. J. Jin, Design strategy for ferroelectric-based polar metals with dimensionality-tunable electronic states, *Sci. China-Phys. Mech. Astron.* **61**, 097011 (2018), <https://doi.org/10.1007/s11433-018-9245-4>

1 Introduction

Polar metals, also called ferroelectric metals when they were firstly proposed by Anderson and Blount [1] in 1965, have been under intensive investigation [2-20] since LiOsO₃ was discovered in 2013 [2], due to the coexistence of two seemingly incompatible properties, ferroelectric-like polar distortion and metallic conductivity. Breaking the inversion symmetry in polar metals gives rise to a series of properties such as the unconventional Cooper pairing in superconductors [21-23], the magneto-electric effect in polar superconductors [24,25], and unique optical properties [26,27]. Because of the lack of intrinsic polar metals, it is imperative

to design easy-realizable polar metals for further research and practical applications. The most widely accepted design rule relies on the “weak-coupling” mechanism proposed by Puggioni and Rondinelli [4] in 2014. Later, the “geometric design” method was developed by Kim et al. [14] in 2016, which is to induce polar distortion in a metal essentially.

An alternative approach to the geometric design is doping a ferroelectric material [20], which leaves room for a wide choice due to the enormous candidate ferroelectrics and metals. We predicted that lone-pair ferroelectrics would have been promising [12,18] and realized the polar metal phase in PbTi_{0.88}Nb_{0.12}O₃ [16]. However, lead compounds suffer fabrication difficulties and environmental issues [28]. Therefore, environmental friendly ferroelectrics such as BaTiO₃ (BTO) deserve much more attention for the design of polar

*Corresponding author (email: kjin@iphy.ac.cn)

metals. Earlier experimental studies on Nb-doped BTO thin films mostly focused on the metal-insulator transitions [29,30]. More recently, some researches have tried to gain insights into the interaction between mobile carriers and ferroelectricity. However, theoretical works [31,32] indicated that the doping in BTO suppresses the polar distortion. So far, experimental attempts have not provide solid proof that polar phase and metallicity can coexist in Nb-doped BTO [33,34] or in oxygen-deficient BTO bulk (BaTiO_{3-δ}) [35,36]. Thus, the coexistence of ferroelectric-like distortion and metallicity in BTO has remained undemonstrated until very recently, when Takahashi et al. [19] reported that the polar metal phase in La-doped BTO thin films epitaxially grown on GaScO₃ substrates. However, disorder and lattice distortions may be introduced by chemical doping and further induce defects or detrimentally affect the polar distortion, resulting in a more likely localization of doping electrons. For example, most of Nb-doped BTO synthesized in previous studies showed insulating or semiconducting behavior [29,30,37-39]. Thus, the progress for obtaining BTO-based polar metal phase by chemical doping is restricted. On the other hand, the problems given by chemical doping can be avoided by adopting the electrostatic doping method. In 2016, Raghavan et al. [34] realized a three-layer prototype structure to electrostatically dope BTO. However, the electrostatic doping is not sufficiently effective because the doping carriers from the carrier reservoir layer (SmTiO₃ and polar interface between SmTiO₃ and BTO) may not reside in the BTO layer. Therefore, it is important to develop more effective electrostatic doping approaches. In addition, very recently, we have suggested that the in-plane compressive strain could help stabilizing the polar metal phase in BTO [20]. Nevertheless, the experimental realization of electrostatic doping combined with strain engineering remains challenging.

In this paper, a multilayer design strategy for obtaining the ferroelectric-based polar metals (FEPs), which is configured as ferroelectric layer/carrier reservoir layer/isolation layer/substrate, is proposed to achieve strain engineering and, more importantly, simultaneous effective electrostatic doping in the ferroelectric material. The polar metal property of this multilayer structure is proved by density functional theory (DFT) calculations. By using BTO as example, detailed investigations on the dimensionality of doping electronic states tuned by the compressive strain and the BTO thickness are also reported, as well as the corresponding high anisotropy of electrical and electronic thermal conductivity.

2 Computational details

DFT calculations were performed within the generalized

gradient approximation (GGA) with the Perdew-Burke-Ernzerhof revised for solids (PBEsol) exchange and correlation functional [40] as implemented in the Vienna *ab initio* simulation package (VASP) [41]. The projector augmented wave method (PAW) [42,43] was used with the following electronic configurations: 4s²4p⁶5s² (Sr), 5s²5p⁶6s² (Ba), 5d¹⁰6s²6p² (Pb), 3s²3p⁶3d²4s² (Ti), 4p⁶4d³5s² (Nb), and 2s²2p⁴ (O). A 520 eV energy cutoff of the plane-wave basis set was used for all calculations. We imposed as a constraint of the in-plane lattice constant $a = b$ to simulate the bi-axial strain under thin-film epitaxial growth on a substrate with a square lattice net. The vacuum was about 20 Å in the slab calculations. For structure optimizations, atomic positions were considered relaxed for energy differences up to 1×10^{-6} eV and all forces were smaller than 1 meV Å⁻¹. During structure relaxations of the modeled multilayer structure, $10 \times 10 \times 1$ gamma-centered k -point meshes were used. During the relaxation of bulk BTO unit cell with various electrostatic doping concentrations for the transport properties calculation, $11 \times 11 \times 11$ gamma-centered k -point meshes were used, while the doping electrons were introduced to the system with a uniform and positive background to achieve charge neutrality. Denser k -point meshes were used for density of states (DOS) calculations.

The Fermi surface was calculated using the Wannier90 [44] code. For the transport properties calculation, we used the Boltzmann transport theory [45] within the constant scattering time (τ) approximation as implemented in the BoltzWann [46] module of the Wannier90 code. We performed a non-self-consistent band-structure interpolation with a dense sampling of $40 \times 40 \times 40$, using the calculated one unit-cell (u.c.) bulk structure of BTO with various electrostatic doping concentrations. The electrical conductivity (σ) and the electronic thermal conductivity (κ^e) require a known value of τ , which was set to 10 fs in all the transport calculations [4,46]. The electronic thermal conductivity needs to be calculated outside the Wannier90 code using its output results [46]. The atomic structures and isosurfaces of the charge density were visualized using the VESTA package [47].

3 Results and discussion

3.1 Multilayer design strategy

Figure 1(a) shows the diagram of the multilayer design strategy, which is composed of a ferroelectric (FE) layer, a carrier reservoir (CR) layer, an isolation (IL) layer, and a substrate. The CR layer can be a metal, or an insulator producing polar discontinuity [48] with the FE layer, so that it is able to electrostatically dope the FE layer and form a polar metal phase. In addition, the FE and CR layer can switch places. Here, the FE layer is placed on the top because this

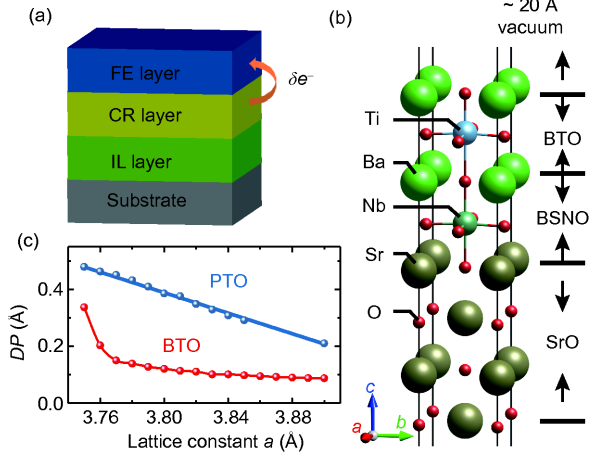


Figure 1 (Color online) (a) Diagram of the multilayer design strategy for the FEPM. (b) Atomic model of the FEPM for the DFT simulations. (c) DP of PbTiO_3 (PTO) and BaTiO_3 (BTO) as functions of the in-plane lattice constant a . Both PTO and BTO are 1 u.c. thick.

configuration is convenient for the experimental study and the application in devices. It is imperative to add the IL layer for preventing the charge transfer from the CR layer to the substrate and, hence, ensuring that the CR layer dopes exclusively the FE layer. Moreover, various strains can be provided by choosing appropriate substrate materials. Therefore, with this design strategy, one can impose the desired strain and the electrostatic doping while engineering the FEPM.

To verify the effectivity of this design strategy via DFT simulations, we modeled the atomic structure of the FEPM by choosing SrTiO_3 (STO) as the substrate, SrO as the IL layer, $\text{Ba}_{0.5}\text{Sr}_{0.5}\text{NbO}_3$ (BSNO) as the CR layer, and BTO as the FE layer. For simplicity, the tilt and rotation of oxygen octahedron in BSNO were not considered, because they should be suppressed significantly due to the symmetry constraint of the IL layer and the substrate, and, these effects can be minimized by choosing an appropriate material for the CR layer. Figure S1 in the [Supplementary Information](#) shows that three additional SrO atomic layer provide a thickness sufficient to isolate the charge transfer from the CR layer to the substrate and ensure that the CR layer dopes only the FE layer. Moreover, with the IL layer, the substrate provides just the constraint of the in-plane lattice constant. Therefore, for simplicity, the atomic structure of the multilayer configuration did not include the substrate in the following DFT calculations, as shown in [Figure 1\(b\)](#). The bi-axial strain can be simulated by simply varying the in-plane lattice constant.

As the ferroelectric polarization is an ill-defined quantity in metallic materials, we used the relative displacement of Ti with respect to O in the TiO_2 plane (DP) to represent the polar distortion in BTO. To prove that this design strategy can be generalized for other ferroelectric materials, we also calculated the case of PbTiO_3 (PTO) as FE layer. The results

of the polar distortion for 1 u.c. thick BTO and PTO are both displayed in [Figure 1\(c\)](#); DP of PTO increases almost linearly with decreasing the in-plane lattice constant a , while that of BTO exhibits an abrupt increase with decreasing a below 3.77 Å. The polar distortion is larger in PTO because the weak-coupling mechanism is naturally satisfied in lone-pair ferroelectrics [12,18], while the abrupt increase of DP in BTO is due to the doping concentration shifting into the weak-coupling region when a is small enough [20]. More importantly, the results clearly demonstrate that 1 u.c. thick BTO and PTO both exhibit remarkable Ti off-centering, which should extend the applications of FEPMs in ultra-thin devices.

3.2 Dimensionality-tunable electronic states

The design strategy proposed resulted to be capable of manipulating the dimensionality of the electronic states in BTO. Before a detailed description, we present the quasi-2D electronic states associated with the polar metal phase in the weak-coupling region of BTO [20] and the mechanism involved.

As shown in [Figure 2\(a\)](#), for doping concentrations below 0.05 $e/u.c.$ in fully relaxed bulk BTO (in the weak-coupling region), the doping electrons distribute only in the Ti d_{xy} orbital and show a quasi-2D feature [20]. With increasing the doping concentration, the electronic states of the doping electrons gradually become isotropic, approximating a 3D feature. To quantify the extent of the anisotropy of the quasi-2D electronic states at low doping, we calculated σ and κ^e at an absolute temperature T of 300 K (room temperature). We defined the anisotropy as the ratio of the xx (yy) component to the zz component of the corresponding conductivity. The xx (yy) and zz components of σ and κ^e in fully relaxed BTO (upper panels) and strained BTO (lower panels, with a of 3.9 Å imposing a compressive strain), respectively, with a doping concentration of 0.05 $e/u.c.$ are plotted in [Figure 2\(b\)](#) and (c); both σ and κ^e around the Fermi level are highly anisotropic. At room temperature, the anisotropy is around tens in fully relaxed BTO and is enlarged by 3-5 times reaching values over fifty in strained BTO with a being 3.9 Å. Moreover, comparing the upper and lower panels in [Figure 2\(b\)](#) and (c), the range of the chemical potential accompanied with highly anisotropic conductivity properties is also strikingly extended. Therefore, both the anisotropy of the conductivity around the Fermi level and the range of chemical potential for maintaining the high anisotropy are remarkably enlarged by the in-plane compressive strain, indicating that the dimensionality of the doping electronic states can be reshaped by strain engineering. In addition, the anisotropy is strongly dependent on the temperature. From [Figure S2](#) in the [Supplementary Information](#), we can see that the anisotropy is enlarged by 2-3 times when the temperature

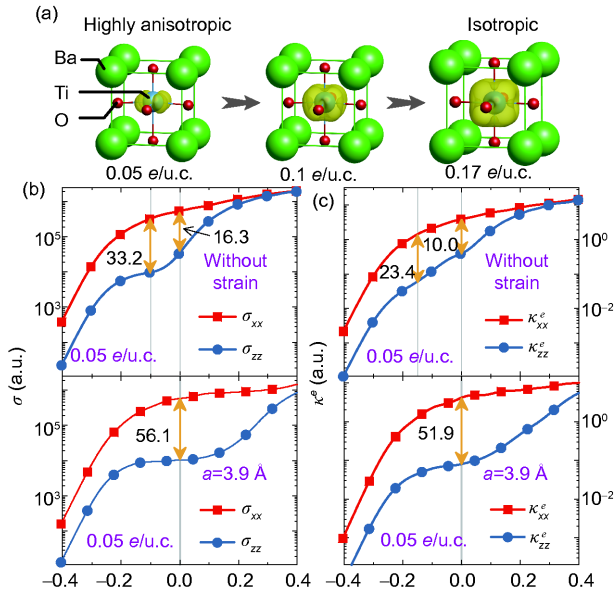


Figure 2 (Color online) (a) Isosurfaces for the charge density of the doping electrons with various doping concentrations in fully relaxed bulk BTO. xx and zz components of the electrical conductivity σ (b) and the electronic thermal conductivity κ^e (c) in fully relaxed BTO (upper panels) and strained BTO (lower panels, with $a = 3.9 \text{ \AA}$), with a doping concentration of 0.05 e/u.c. and $T=300 \text{ K}$.

is cooled down to 100 K .

To understand the mechanism causing the highly anisotropic conductivity of the quasi-2D electronic states, we present in **Figure 3** the Fermi surface and the band structure of Ti d_{xy} state along \mathbf{k}_x and \mathbf{k}_z directions in the fully relaxed bulk BTO with the 0.05 e/u.c. doping concentration. The Fermi surface contains states only from the d_{xy} orbital because of the low doping concentration. As shown in **Figure 3(a)**, the Fermi surface exhibits a highly anisotropic feature; it is nearly isotropic in the $(\mathbf{k}_x, \mathbf{k}_y)$ plane and is cut by the first Brillouin zone (BZ) border along the $\Gamma \rightarrow \mathbf{k}_z$ orientation. The Fermi surface separates occupied electronic states from unoccupied ones at zero temperature. Hence, its anisotropy observed in **Figure 3(a)** means that the electronic states whose momentum has only the \mathbf{k}_z component are all occupied. This scenario can be better demonstrated by the band structure shown in **Figure 3(b)**. The d_{xy} band along the $\Gamma \rightarrow \mathbf{k}_z$ direction is entirely below the Fermi level, thus the electrons with only the \mathbf{k}_z component do not contribute to the conductivity. Meanwhile, the Fermi level cuts across the d_{xy} band along the $\Gamma \rightarrow \mathbf{k}_x$ direction, indicating that the electrons whose momentum has only the \mathbf{k}_x component are conductive. Therefore, the conductivity along the z direction is significantly suppressed, leading to the high anisotropy of σ and κ^e . The quasi-2D feature of the electronic states at the Fermi level originates from the intrinsic symmetry of the d_{xy} orbital, which is essentially different from the 2DEG within insulator interfaces [48].

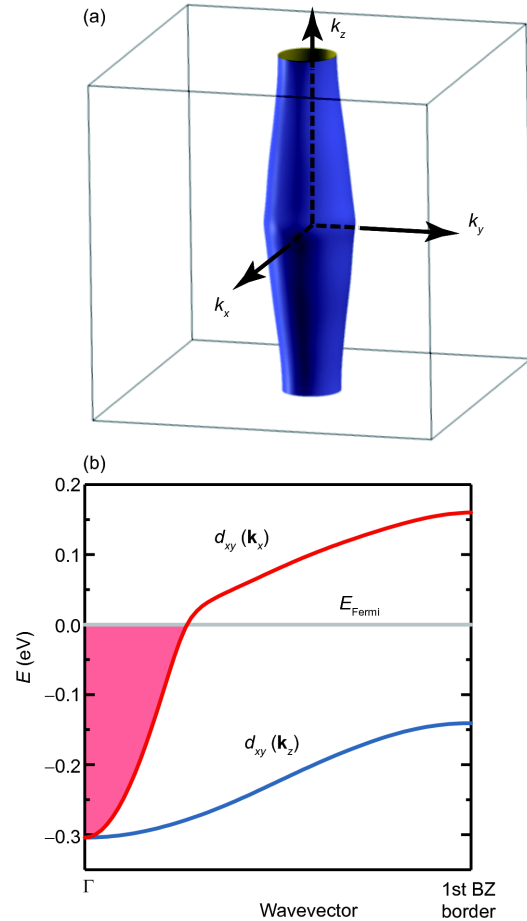


Figure 3 (Color online) Fermi surface (a) and band structure of Ti d_{xy} state (b) in fully relaxed bulk BTO with the 0.05 e/u.c. doping concentration.

3.3 Strain and thickness engineering

To demonstrate that strain and thickness can be used to tune the dimensionality of the doping electronic states in our proposed structure, in **Figures 4(a-c)** we plot the isosurfaces for the partial charge density integrated from the conduction band minimum (CBM) into the Fermi level with various strains and thicknesses of BTO. Here, we focus only on the electronic states in BTO because polar distortion may not emerge in the CR layer, although its lattice may be softened by the FE layer [49]. Also, as seen in the last section, when the doping level is within the weak-coupling region [20], the quasi-2D d_{xy} states exhibit highly anisotropic conductivity. Increasing the doping introduces more d_{yz}/d_{xz} electronic states, making the charge distribution of doping electrons less anisotropic and the lattice less polar distorted. By comparing **Figure 4(b)** with **Figure 4(a)**, it can be seen that the electronic states in BTO become more anisotropic by reducing a , indicating that larger compressive strains can enhance the transport anisotropy and make the electronic states more 2D-featured. This can be understood considering

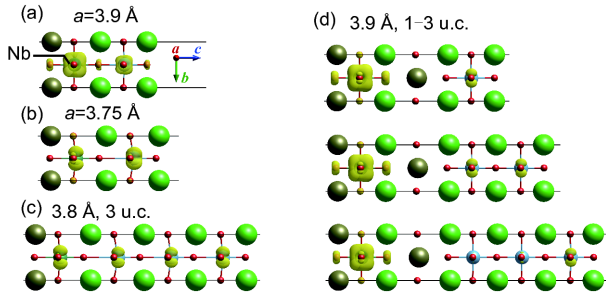


Figure 4 (Color online) (a)-(c) Isosurfaces for the partial charge density integrated from the CBM into the Fermi level with various strains and thicknesses of BTO. Only the BSNO/BTO part of the polar metal structure is shown. (d) Partial charge density distributions the same as those in (a)-(c), but in the BSNO/SrO/BTO part with different thicknesses of BTO. In (a)-(d), the isosurface levels are using the same value of $0.02 e \text{ \AA}^{-3}$.

that the compressive strain enlarges the weak-coupling region [20] and thereby increases the polar distortion and the proportion of d_{xy} states. By comparing Figure 4(a) and (c), it can be seen that by increasing the thickness of BTO and decreasing a , the electronic states are reduced to quasi-2D ones, which results from the decreased doping concentration and the increased compressive strain. Therefore, electronic states with tunable dimensionality can be engineered by strain and BTO thickness.

However, their engineering by the thickness of BTO is much complicated because the polarization effect which modulates the surface conductivity of the FEPM [50] if the BTO layer is thick enough, assuming that polarization and metallicity can coexist. Naturally, the BSNO transfers electrons into BTO and forms a built-in electric field (E_{bi}) pointing toward BTO. If polarization does not occur in BTO as in a regular heterointerface, the transferred electrons distribute around the interface and form an insulating surface. A polarization against E_{bi} reduces the charge transfer and confines the transferred electrons within the interface area, leaving an insulating surface as well, while a polarization along E_{bi} drives more electrons from BSNO to BTO and forms a conductive surface. However, although E_{bi} enhances the Ti displacement away from BSNO, it also leads to a considerable charge transfer, preventing the quasi-2D electronic states. Moreover, a considerable charge transfer requires a ferroelectric layer thick enough to exhibit polarization and surface conductivity. To reduce the influence of the direct contact between BSNO and BTO, we inserted an additional IL layer to effectively reduce the charge transfer. As shown in the upper panel of Figure 4(d), the charge transfer is successfully reduced compared with Figure 4(a) by inserting an additional SrO atomic layer. The DOS presented in Figure S3 in the Supplementary Information show that the doping electrons distribute only in the quasi-2D featured d_{xy} orbital, further proving that 1 u.c. thick BTO can produce quasi-2D electronic states. Moreover, DFT

calculations reveal that, with the additional SrO layer, a BTO thickness of 3 u.c. is enough to provide a conductive surface and a nearly insulating interface, as shown in the lower panel of Figure 4(d). More importantly, the conductive surface indicates the coexistence of polarization and metallicity. The polarization is naturally aligned against the built-in electric field under its same influence to reduce the electrostatic energy. Therefore, the thickness of BTO, as demonstrated above, not only reshapes the doping electrons, but also modifies their spatial distribution. Furthermore, this suggests that the coexistence of polar distortion and free carriers acts in a complicated and unusual behavior, which is closely related to the doping concentration and the thickness of the material if the polar distortion is z -oriented. Given the above described properties, polar metals may be helpful for designing ultra-thin, ultrafast and low-power switch devices, thanks to the high on/off ratio of ferroelectric materials and their polarization-dependent surface conductivity.

4 Conclusion

A multilayer design strategy, configured as ferroelectric layer/CR layer/isolation layer/substrate, has been proposed to electrostatically dope ferroelectric materials in an effective way for obtaining FEPMs. DFT calculations demonstrated that the ferroelectric-like polar distortion in the ultra-thin ferroelectric layer of our proposed design is considerably preserved, which should extend the application of polar metals in ultra-thin devices. The multilayer structure achieved the electrostatic doping in the ferroelectric layer more effectively by annihilating the charge transfer from the CR layer to the substrate. The strain can be imposed conveniently by selecting the proper substrate, which should promote the research combined with both strain and electrostatic doping effects. We also observed that the in-plane compressive strain and the thickness of BTO can affect the dimensionality of the doping electronic states in BTO, which is accompanied by the modulation of the anisotropy of electrical and electronic thermal conductivity. More importantly, we confirmed that the polarization and the metallicity coexist in this multilayer structure.

This design strategy is easy to realize, which is an advantage for further exploring the physical properties of polar metals and understanding the long-standing dispute about whether polar distortion and free carriers can coexist in BTO. With their fascinating properties, polar metals are expected to show extraordinary performances when applied in innovative nanoscale electronic and thermoelectric devices.

This work was supported by the National Key Basic Research Program of China (Grant No. 2014CB921001), the Strategic Priority Research Program (B) of the Chinese Academy of Sciences (Grant No. XDB07030200),

the Key Research Program of Frontier Sciences of the Chinese Academy of Sciences (Grant No. QYZDJ-SSW-SLH020), the National Key Research and Development Program of China (Grant No. 2017YFA0303604), and the National Natural Science Foundation of China (Grant Nos. 11721404, and 11674385).

Supporting Information

The supporting information is available online at phys.scichina.com and www.springerlink.com. The supporting materials are published as submitted, without typesetting or editing. The responsibility for scientific accuracy and content remains entirely with the authors.

- 1 P. W. Anderson, and E. I. Blount, *Phys. Rev. Lett.* **14**, 217 (1965).
- 2 Y. Shi, Y. Guo, X. Wang, A. J. Princep, D. Khalyavin, P. Manuel, Y. Michiue, A. Sato, K. Tsuda, S. Yu, M. Arai, Y. Shirako, M. Akaogi, N. Wang, K. Yamaura, and A. T. Boothroyd, *Nat. Mater.* **12**, 1024 (2013), arXiv: 1509.01849.
- 3 G. Giovannetti, and M. Capone, *Phys. Rev. B* **90**, 195113 (2014), arXiv: 1404.7705.
- 4 D. Puggioni, and J. M. Rondinelli, *Nat. Commun.* **5**, 3432 (2014), arXiv: 1310.1148.
- 5 H. Sim, and B. G. Kim, *Phys. Rev. B* **89**, 201107(R) (2014), arXiv: 1311.4139.
- 6 H. J. Xiang, *Phys. Rev. B* **90**, 094108 (2014), arXiv: 1312.4225.
- 7 C. He, Z. Ma, B. Z. Sun, Q. Li, and K. Wu, *Comput. Mater. Sci.* **105**, 11 (2015).
- 8 H. M. Liu, Y. P. Du, Y. L. Xie, J. M. Liu, C. G. Duan, and X. Wan, *Phys. Rev. B* **91**, 064104 (2015), arXiv: 1409.4953.
- 9 D. Puggioni, G. Giovannetti, M. Capone, and J. M. Rondinelli, *Phys. Rev. Lett.* **115**, 087202 (2015), arXiv: 1503.01948.
- 10 N. A. Benedek, and T. Birol, *J. Mater. Chem. C* **4**, 4000 (2016).
- 11 A. Filippetti, V. Fiorentini, F. Ricci, P. Delugas, and J. Íñiguez, *Nat. Commun.* **7**, 11211 (2016), arXiv: 1511.09312.
- 12 X. He, and K. Jin, *Phys. Rev. B* **94**, 224107 (2016), arXiv: 1603.07418.
- 13 F. Jin, A. Zhang, J. Ji, K. Liu, L. Wang, Y. Shi, Y. Tian, X. Ma, and Q. Zhang, *Phys. Rev. B* **93**, 064303 (2016), arXiv: 1703.02701.
- 14 T. H. Kim, D. Puggioni, Y. Yuan, L. Xie, H. Zhou, N. Campbell, P. J. Ryan, Y. Choi, J. W. Kim, J. R. Patzner, S. Ryu, J. P. Podkaminer, J. Irwin, Y. Ma, C. J. Fennie, M. S. Rzechowski, X. Q. Pan, V. Gopalan, J. M. Rondinelli, and C. B. Eom, *Nature* **533**, 68 (2016).
- 15 I. Lo Vecchio, G. Giovannetti, M. Autore, P. Di Pietro, A. Perucchi, J. He, K. Yamaura, M. Capone, and S. Lupi, *Phys. Rev. B* **93**, 161113(R) (2016), arXiv: 1509.01785.
- 16 J. Gu, K. Jin, C. Ma, Q. Zhang, L. Gu, C. Ge, J. Wang, C. Wang, H. Guo, and G. Yang, *Phys. Rev. B* **96**, 165206 (2017), arXiv: 1706.04855.
- 17 X. Jing, W. Xu, C. Yang, J. Feng, A. Zhang, Y. Zeng, M. Qin, M. Zeng, Z. Fan, J. Gao, X. Gao, G. Zhou, X. Lu, and J. M. Liu, *Appl. Phys. Lett.* **110**, 182903 (2017).
- 18 C. Ma, X. He, and K. Jin, *Phys. Rev. B* **96**, 035140 (2017).
- 19 K. S. Takahashi, Y. Matsubara, M. S. Bahramy, N. Ogawa, D. Hashizume, Y. Tokura, and M. Kawasaki, *Sci. Rep.* **7**, 4631 (2017).
- 20 C. Ma, K. Jin, C. Ge, and G. Yang, *Phys. Rev. B* **97**, 115103 (2018).
- 21 V. M. Edelstein, *J. Phys.-Condens. Matter* **8**, 339 (1996).
- 22 E. Bauer, H. Kaldarar, R. Lackner, H. Michor, W. Steiner, E. W. Scheidt, A. Galatanu, F. Marabelli, T. Wazumi, K. Kumagai, and M. Feuerbacher, *Phys. Rev. B* **76**, 014528 (2007).
- 23 E. Bauer, G. Rogl, X. Q. Chen, R. T. Khan, H. Michor, G. Hilscher, E. Royanian, K. Kumagai, D. Z. Li, Y. Y. Li, R. Podloucky, and P. Rogl, *Phys. Rev. B* **82**, 064511 (2010), arXiv: 1007.0420.
- 24 V. M. Edelstein, *Phys. Rev. Lett.* **75**, 2004 (1995).
- 25 V. M. Edelstein, *Phys. Rev. B* **72**, 172501 (2005).
- 26 V. P. Mineev, and Y. Yoshioka, *Phys. Rev. B* **81**, 094525 (2010), arXiv: 1001.2113.
- 27 V. M. Edelstein, *Phys. Rev. B* **83**, 113109 (2011).
- 28 K. J. Choi, M. Biegalski, Y. L. Li, A. Sharan, J. Schubert, R. Uecker, P. Reiche, Y. B. Chen, X. Q. Pan, V. Gopalan, L. Q. Chen, D. G. Schlom, and C. B. Eom, *Science* **306**, 1005 (2004).
- 29 L. Liu, H. Guo, H. Lü, S. Dai, B. Cheng, and Z. Chen, *J. Appl. Phys.* **97**, 054102 (2005).
- 30 Y. Shao, R. A. Hughes, A. Dabkowski, G. Radtke, W. H. Gong, J. S. Preston, and G. A. Botton, *Appl. Phys. Lett.* **93**, 192114 (2008).
- 31 Y. Iwazaki, T. Suzuki, Y. Mizuno, and S. Tsuneyuki, *Phys. Rev. B* **86**, 214103 (2012).
- 32 Y. Wang, X. Liu, J. D. Burton, S. S. Jaswal, and E. Y. Tsymal, *Phys. Rev. Lett.* **109**, 247601 (2012), arXiv: 1208.5830.
- 33 K. Page, T. Kolodiazny, T. Proffen, A. K. Cheetham, and R. Seshadri, *Phys. Rev. Lett.* **101**, 205502 (2008), arXiv: 0808.1308.
- 34 S. Raghavan, J. Y. Zhang, O. F. Shoron, and S. Stemmer, *Phys. Rev. Lett.* **117**, 037602 (2016).
- 35 T. Kolodiazny, M. Tachibana, H. Kawaji, J. Hwang, and E. Takayama-Muromachi, *Phys. Rev. Lett.* **104**, 147602 (2010).
- 36 I. K. Jeong, S. Lee, S. Y. Jeong, C. J. Won, N. Hur, and A. Llobet, *Phys. Rev. B* **84**, 064125 (2011).
- 37 D. Nagano, H. Funakubo, K. Shinozaki, and N. Mizutani, *Appl. Phys. Lett.* **72**, 2017 (1998).
- 38 M. Nasir Khan, H. T. Kim, T. Kusawake, H. Kudo, K. Ohshima, and H. Uwe, *J. Appl. Phys.* **86**, 2307 (1999).
- 39 N. Lemée, C. Dubourdieu, G. Delabouglise, J. P. Sénateur, and F. Laroudie, *J. Cryst. Growth* **235**, 347 (2002).
- 40 J. P. Perdew, A. Ruzsinszky, G. I. Csonka, O. A. Vydrov, G. E. Scuseria, L. A. Constantin, X. Zhou, and K. Burke, *Phys. Rev. Lett.* **100**, 136406 (2008), arXiv: 0707.2088.
- 41 G. Kresse, and J. Furthmüller, *Phys. Rev. B* **54**, 11169 (1996).
- 42 P. E. Blöchl, *Phys. Rev. B* **50**, 17953 (1994).
- 43 G. Kresse, and D. Joubert, *Phys. Rev. B* **59**, 1758 (1999).
- 44 A. A. Mostofi, J. R. Yates, G. Pizzi, Y. S. Lee, I. Souza, D. Vanderbilt, and N. Marzari, *Comput. Phys. Commun.* **185**, 2309 (2014).
- 45 N. W. Ashcroft, and N. D. Mermin, *Solid State Physics* (Thomson Learning, Inc., Stamford, 1976).
- 46 G. Pizzi, D. Volja, B. Kozinsky, M. Fornari, and N. Marzari, *Comput. Phys. Commun.* **185**, 422 (2014), arXiv: 1305.1587.
- 47 K. Momma, and F. Izumi, *J. Appl. Cryst.* **41**, 653 (2008).
- 48 A. Ohtomo, and H. Y. Hwang, *Nature* **427**, 423 (2004).
- 49 G. Gerra, A. K. Tagantsev, N. Setter, and K. Parlinski, *Phys. Rev. Lett.* **96**, 107603 (2006).
- 50 C. Ge, K. J. Jin, C. Wang, H. B. Lu, C. Wang, and G. Z. Yang, *Appl. Phys. Lett.* **99**, 063509 (2011).